2020 IEEE International Conference on Robotics and Automation (ICRA)
31 May - 31 August, 2020. Paris, France

On the efficient control of series-parallel compliant articulated robots

Vishnu Dev Amara[1], Jörn Malzahn[1], Zeyu Ren[1], Wesley Roozing[2] and Nikos Tsagarakis[1]

***Abstract*— Torque distribution in redundant robots that combine the potential of asymmetric series-parallel actuated branches and multi-articulation pose a non-trivial challenge. To address the problem, this work proposes a novel optimization based controller that can accommodate various quadratic criteria to perform the torque distribution among dissimilar series and parallel actuators in order to maximize the motion efficiency. Three candidate criteria are composed and their performances are compared during periodic squat motions with a 3 degree of freedom series-parallel compliant articulated leg prototype. It is first shown that by minimizing a criterion that takes into account the actuator hardware specifications such as torque constant and transmission ratio, the gravity-driven phases can be lengthened. Thereby, this particular criterion results in slightly better performance than when adopting a strategy that maximizes the torque allocation to the higher efficiency actuators. Furthermore, valuable insights such as that the efficacy of maximum utilization of the highly-efficient parallel actuation branches decreases progressively at high frequencies were observed.**

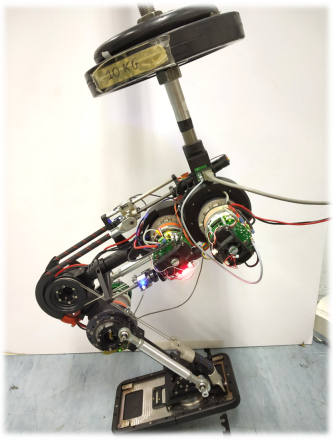

Fig. 1. The articulated leg prototype used in this work.

I. Introduction

Extending the power autonomy of robotic systems is fundamental for their successful deployment in applications where they are expected to be capable of prolonged untethered operation. Such a requirement can be addressed only through advancements in robot efficiency through more efficient, actuation and motion control strategies. Research on actuation systems towards this objective has already led to a radical departure from stiff to compliant actuators. Compliant actuators are inherently robust, efficient, safer and can potentially satisfy peak velocity/power achievements. Compliant actuation technology has spawned two broad classes of actuators - series elastic actuators (SEA) and parallel elastic actuators (PEA). SEAs utilize soft elements in series with the motor while PEAs recruit soft elements in parallel with the main actuation drive. While SEAs have matured to be the preferred drive units in many contemporary high-performance robots [1], [2], [3], PEAs have not attracted equal attention although they have shown massive energy-efficiency benefits [4], [5], [6], [7]. Further, it is not fully understood how to combine the two classes of actuators for achieving high performance and energy-efficiency. In [8], the authors demonstrated a method to synergistically employ them both to obtain efficient motion. An asymmetric joint unit that comprises a high power SEA for primary torque supply along with a high efficiency PEA for energy storage/release led to considerable power savings.

[1]V. D. Amara, J. Malzahn, Z. Ren and N. Tsagarakis are with the Humanoids and Human-centered Mechatronics Lab, Istituto Italiano di Tecnologia, Genova, Italy (e-mail: vishnu.amara@iit.it). [2]W. Roozing is with University of Twente, the Netherlands.

Moreover, in biological systems, muscle units can span multiple joints and enable energy efficiency and power transfer between the spanned joints [9], [10], [11]. Coupling this principle along with the aforementioned idea of an asymmetric joint unit, the authors of [12], [13] optimized and developed a three degrees of freedom (DoF) leg prototype, the eLeg. Additionally, the PEAs in the eLeg can be swiftly reconfigured to either encompass one or two joints displaying distinct articulation topologies. With the PEAs providing for gravity load cancellation/majority of the torque demand in steady-state, the monoarticulated and biarticulated configurations exhibited substantial energy savings [14], [15].

Nevertheless, a research gap exists in understanding how to optimally distribute the desired torques among the primary and the secondary actuator units. The authors of [16] compared various approaches to resolve the torques from identical biarticular actuators among the various joints in a redundant manipulator. The question still remains open when actuators of different efficiency and torque capacity are employed on distinct articulation topologies. An investigation into the same taking into account the hardware specifications can lead to valuable considerations for control.

Therefore, this article investigates the efficiency of various torque-distribution strategies in compliant articulated robots powered by hybrid series and parallel actuation principles. Firstly, a novel optimization based torque distribution framework that can apportion the instantaneous joint torque demand to the various torque sources based on different criteria are presented. Secondly, we investigate if demanding maximum torques from the higher efficiency parallel actuators is the best strategy, especially during periodic motions with

978-1-7281-7395-5/20/$31.00 ©2020 IEEE

significant gravity-driven phases, by performing experiments on the 3-DoF leg setup depicted in Fig.1 using cyclic squat motions on two different articulation topologies. Thirdly, we extend our energy-based analysis to squat motions across various frequencies to obtain some valuable insights for energy-efficient joint torque resolution.

The paper is organized as follows. A brief overview of the actuation branches, the leg prototype and its modelling are provided in Sec. II. The derivation of the control framework based on the various cost functions is described in Sec. III. An analysis is conducted with experiments and a discussion is presented in Sec. IV. The paper finally concludes in Sec. V providing valuable recommendations for future work.

II. Background

A. Articulated Compliant Actuation (ACA) Arrangements

The ACA arrangement that we refer to in this paper comprise compliant actuators of vastly different torque output capacity, efficiency and stiffness characteristics. The motor M1 is a SEA that is capable of exerting high power and forms the power branch (PB). Motor M2 is a low power motor that utilizes a ball-screw transmission mechanism of a high rotary - linear reduction. The transmission unit is coupled to the driven joints via elastic tendons and forms the energy storage branch (ESB). While the efficiency and energy storage capacity of the ESB is quite high, their stiffness is quite small compared to the PB.

Additionally, the ACA branches are modular and can exhibit more than a single articulation topology. When monoarticulated, the ESB tendon is directly coupled to a single joint while in multiarticulation, the same spans over two or more joints through free pulleys and is then coupled to a distal joint. In the latter case, the elongation of the ESB tendon transmits torque to both the spanned as well as the driven joint. Consequently, the ESB torque profile depends on the joint configuration, pulley radii and tendon stiffness.

B. eLeg Hardware with ACA Branches

The eLeg is a three DoF semi-anthropomorphic planar leg prototype. The hip joint is driven exclusively by a SEA; the knee and ankle joints are powered by ACA branches. The ESB units in the eLeg prototype can actively load the tendons to achieve the desired extensions. Further, to demonstrate generality and energy-efficiency characteristics of the prototype, the adjustable ACA branches can be swiftly reconfigured to obtain various configurations. In this paper, we utilize the following articulation topologies, see Fig.2 :

- **noESB** : All joints are solely driven by SEAs and the robot weighs 24.5 kg.
- **Biarticulated** : In this configuration, while the ankle ESB is biarticulated, the knee ESB is monoarticulated. Here, the ESBs serve the function of gastrocnemius and lateralis muscles and the robot weighs 26.1 kg.

The SEAs on the eLeg are all Kollmorgen TBMS-6025 motors that employ CPL-20 Harmonic Drive (HD) gearboxes and are in series with deflection-based torque sensors

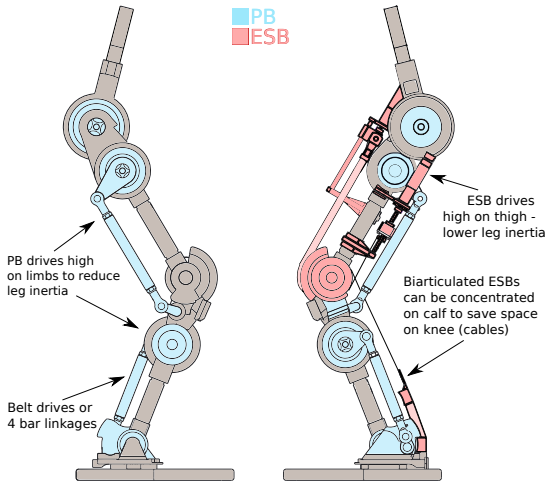

Fig. 2. The *noESB* and the *biarticulated* configurations of the anthropomorphic eLeg with ACA arrangements.

[17][1]. The hip joint is loaded with a 15 kg trunk. The ESBs employ Maxon EC22 motors with Maxon GP22 HP planetary gearboxes. For the tendons, we utilize rubber-type bungee cords that showcase S-shaped stiffness curves. The bungees are unidirectional, i.e. they transmit forces only when stretched. We allow for elongations up to 80% of their natural lengths. Strain gauges attached on the ballscrew nuts provide for tendon force measurement. Stiffness coefficients are computed in the working range of the bungees through linear regression. Necessary specifications for the PB and ESB units are tabulated in Table I. For more details about the mass, length and hardware specifications, refer to [18], [19].

C. ACA Actuation Modelling

For an n joint articulated floating-base planar robot with $n+3$ DoF and m ACA branches the tendon deflections $\Delta \in \mathbb{R}^n$, can be written :

$$\Delta = \mathbf{S}\mathbf{p} + \mathbf{T}\mathbf{q}. \tag{1}$$

where $\mathbf{q} \in \mathbb{R}^n$ is the joint configuration vector and $\mathbf{p} \in \mathbb{R}^m$ is the tendon pretension vector[2]. $\mathbf{S} \in \mathbb{R}^{nxm}$ is a selection matrix that indicates the joints equipped with ACA branches. $\mathbf{T} \in \mathbb{R}^{nxn}$ is a topology matrix and relates the rotary joint configurations to the linear deflections of the coupled tendons. The

[1]TREE Robotics, treerobotics.eu/

[2]Without loss of generality, we assume $m \leq n$, i.e. ACA branches can either be present in some or all of the joints.

TABLE I
eLeg specifications

Specification	PB	ESB
Transmission Ratio	80	6.66e4 (Knee), 3.64e4 (Ankle)
Stiffness	5.8 kNm/rad	7.8 kN/m (Knee), 29.5 kN/m (Ankle bi)
Torque constant	85 mNm/A	14.2 mNm/A
Winding resistance	0.318 ohm	0.797 ohm

topology matrix $\mathbf{T}$ is a function of the tendon transmission ratios (pulley radii), see [19]. The forces due to the tendon deflection can be approximated :

$$\mathbf{F_p} = \begin{cases} \mathbf{K}\Delta, & \Delta > 0, \\ 0, & \Delta \leq 0. \end{cases} \tag{2}$$

where $\mathbf{K} \in \mathbb{R}^{nxn}$ is a stiffness matrix whose diagonal elements are the linear stiffnesses of the unidirectional bungees. Then by using the same topology matrix again, the tendon forces can be mapped to the joint torques :

$$\boldsymbol{\tau_p} = -\mathbf{T^T F_p} = -\mathbf{T^T K}(\mathbf{Sp} + \mathbf{Tq}). \tag{3}$$

Finally, the total instantaneous joint torque vector can be written as the sum of the torques due to PB and ESB :

$$\boldsymbol{\tau} = \boldsymbol{\tau}_{PB} + \boldsymbol{\tau}_p \,. \tag{4}$$

III. Optimization based torque resolution

Resolving actuator redundancy to apportion the joint torque demand is of paramount importance in redundant robots. Furthermore, with multiarticulation, the ESB torques at the spanned joints depend on the configuration of all the spanned joints. Therefore, resolving the torques among the branches is not straightforward. In this work, we use an online optimization based approach to resolve the commanded instantaneous torques from PB and ESB actuators.

A. Choice of optimization method

More often, the optimization criteria is a quadratic function of certain control variables [20] which might be subjected to linear and box constraints. Owing, to its efficacy and computational efficiency in solving problems online including inverse dynamics [21], trajectory optimization [22], footstep planing [23], etc. we choose to use a quadratic programming (QP) based method [24] to obtain torque commands for the ESBs. In particular, QP algorithm provides for the instantaneous pretension references $\mathbf{p}^\star$. The remaining instantaneous joint torque demand is satisfied by the PB actuators, see Fig. 3. It is worth mentioning that the torque distribution scheme is completely privy to the higher level control strategy.

B. Cost function candidates

We consider the following cost functions in this work :

1) Maximize ESB load share (MELS): In [15], [19], the controller minimizes the squared norm of the error between the commanded joint torque and the ESB load torque. Although the high-efficiency ESBs cannot solely satisfy the joint torque requirements in the eLeg, they can surpass the gravitational load torques which happen to be the most significant during slow periodic motions. In this work, we use a similar criterion that aims to allocate the maximum possible torque demand to the ESB :

$$J = (\boldsymbol{\tau}_p - \boldsymbol{\tau}^\star)^T (\boldsymbol{\tau}_p - \boldsymbol{\tau}^\star). \tag{5}$$

where $\boldsymbol{\tau}^\star$ is the joint torque reference vector.

2) Minimize sum of squared load currents (MSLC): A common candidate cost that is frequently used in optimal control to obtain actuator inputs is the minimization of the sum of squared input torques. However, due to the differences in parameters including transmission ratio, motor torque constant, tendon stiffness, the actual electrical effort in delivering the same output torque to the load varies across the non-homogenous actuators. Therefore, we consider a more general criterion, the sum of squared currents that correspond to the load torques :

$$\begin{aligned} J &= \mathbf{i}_{PB}^T \, \mathbf{i}_{PB} + \mathbf{i}_p^T \, \mathbf{i}_p \\ &= (\mathbf{A}_{PB}(\boldsymbol{\tau}_p - \boldsymbol{\tau}^\star))^T \, (\mathbf{A}_{PB} \, (\boldsymbol{\tau}_p - \boldsymbol{\tau}^\star)) + \\ &\quad (\mathbf{A}_p \mathbf{F}_p)^T \, (\mathbf{A}_p \mathbf{F}_p). \end{aligned} \tag{6}$$

where $\mathbf{A}_{PB}$ and $\mathbf{A}_p$ are diagonal matrices given by $\text{diag}\left(\left[({}^{PB}k_{\tau_1} \, {}^{PB}N_1)^{-2}, \ldots, ({}^{PB}k_{\tau_n} \, {}^{PB}N_n)^{-2}\right]\right)$ and $\text{diag}\left(\left[({}^{p}k_{\tau_1} \, {}^{p}N_1)^{-2}, \ldots, ({}^{p}k_{\tau_m} \, {}^{p}N_m)^{-2}\right]\right)$. Here ${}^{(.)}N_{(.)}$ and ${}^{(.)}k_{\tau_{(.)}}$ refer to the transmission ratio and the torque constant of the corresponding actuator.

3) Minimize sum of power losses (MSPL): Further, the dissipated power can vary across unidentical actuators due to their distinct electrical dynamics [25]. Specifically, the electrical winding resistances are not the same across different actuators, therefore the electrical losses associated while generating the same torque output are different. In this work, according to the manufacturer specifications, the winding resistance of the ESB motors are more than twice of the PB motors. Taking this into account, the sum of the electrical power losses associated with only the load torques is considered as a cost function candidate in this work :

$$\begin{aligned} J &= \mathbf{i}_{PB}^T \, \mathbf{R}_{PB} \, \mathbf{i}_{PB} + \mathbf{i}_p^T \, \mathbf{R}_p \, \mathbf{i}_p \\ &= (\mathbf{A}_{PB}(\boldsymbol{\tau}^\star - \boldsymbol{\tau}_p))^T \, \mathbf{R}_{PB} \, (\mathbf{A}_{PB} \, (\boldsymbol{\tau}^\star - \boldsymbol{\tau}_p)) + \\ &\quad (\mathbf{A}_p \mathbf{F}_p)^T \, \mathbf{R}_p \, (\mathbf{A}_p \mathbf{F}_p). \end{aligned} \tag{7}$$

where $\mathbf{R}_{(.)}$ is a diagonal matrix that contains as its elements the resistances of the electrical windings in the actuators of the corresponding branch.

C. QP Problem formulation

In each of the above cases, a QP problem is formulated to obtain the desired pretension references $\mathbf{p}^\star$ that comply with the following constraints :

- *Tendon slack constraints* - since the bungees are unidirectionally elastic, slack in them is unfavourable. Hence, to avoid slack, soft constraints are enforced with the help of slack variables.
- *ESB pretension constraints* - the bungees can only be stretched to a finite extent.
- *ESB velocity constraints* - the ESB actuators have a limit on the maximum achievable linear velocity.

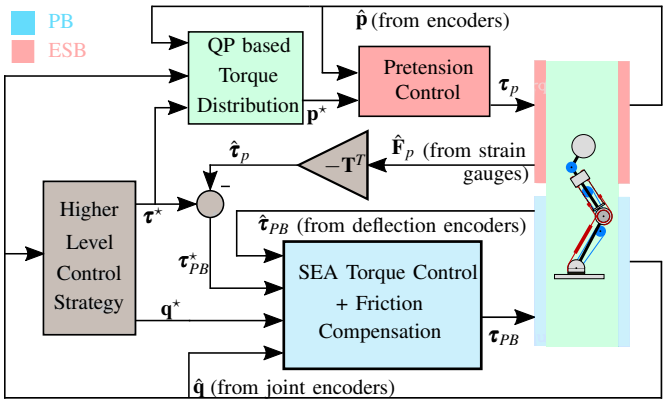

Fig. 3. Schematic of the control architecture on the eLeg.

Consequently, we have the QP problem in discrete form :

$$\begin{aligned} \underset{\mathbf{p}^\star_{i+1},\,\tilde{\mathbf{p}}_{i+1}}{\text{minimize}} \quad & J_{i+1}\left(\mathbf{q}_i, \boldsymbol{\tau}^\star_i, \mathbf{p}^\star_{i+1}, \tilde{\mathbf{p}}_{i+1}\right) \\ \text{subject to} \quad & \mathbf{S}\left(\mathbf{p}^\star_{i+1} + \tilde{\mathbf{p}}_{i+1}\right) + \mathbf{T}\mathbf{q}_i \geq \mathbf{0}, \\ & \underline{\mathbf{p}} \leq \mathbf{p}^\star_{i+1} \leq \bar{\mathbf{p}}, \quad \tilde{\mathbf{p}}_{i+1} \geq \mathbf{0}, \\ & \underline{\dot{\mathbf{p}}}\,\Delta t \leq \mathbf{p}^\star_{i+1} - \mathbf{p}_i \leq \bar{\dot{\mathbf{p}}}\,\Delta t\,. \end{aligned} \tag{8}$$

where $\tilde{\mathbf{p}} \in \mathbb{R}^m$ denotes the slack variable, Δt is the control step size. $\underline{(.)}$ and $\bar{(.)}$ denote the minimum and maximum values of the corresponding quantity. $(.)_i$ and $(.)_{i+1}$ denote the quantity at the current and successive time instants.

While formulating the QP problem, it is sufficient to obtain the quadratic and linear terms associated with the states that are solved for. A single template expression in the QP framework can be converted into the various aforementioned candidate cost functions :

$$\begin{aligned} J_{i+1} = \mathbf{p}^{\star T}_{i+1} & \left(\mathbf{S}^T(\mathbf{C}_{PB}\mathbf{T}_M^T\mathbf{T}_M + \mathbf{S}\mathbf{C}_P\mathbf{S}^T\mathbf{K}^T\mathbf{K})\mathbf{S}\right)\mathbf{p}^\star_{i+1} + \\ & \mathbf{p}^{\star T}_{i+1}\Big(2\,\mathbf{S}^T\Big(\mathbf{C}_{PB}\,\mathbf{T}_M^T(\mathbf{T}_M\mathbf{T}\mathbf{q}_i + \boldsymbol{\tau}^\star_i) + \\ & \mathbf{S}\mathbf{C}_p\mathbf{S}^T\,\mathbf{K}^T\mathbf{K}\mathbf{T}\mathbf{q}_i\Big)\Big) + \tilde{\mathbf{p}}^T_{i+1}\tilde{\mathbf{W}}\tilde{\mathbf{p}}_{i+1}. \end{aligned} \tag{9}$$

where $\mathbf{T}_M$ is $\mathbf{T}^T\,\mathbf{K}$. $\mathbf{C}_{PB} \in \mathbf{R}^{nxn}$ and $\mathbf{C}_p \in \mathbf{R}^{mxm}$ are diagonal matrices of weighting coefficients associated with PB and ESB actuators. $\tilde{\mathbf{W}} \in \mathbf{R}^{mxm}$ is a diagonal weighting matrix for the slack variables. Table II shows how by using (3) and merely setting the weighting coefficient matrices $\mathbf{C}_{PB}$ and $\mathbf{C}_p$ in (9) appropriately, one can formulate the QP problems with the various aforementioned cost functions.

TABLE II

QP PROBLEM FORMULATION - WEIGHTINGS

Optimization criteria	$\mathbf{C}_{PB}$	$\mathbf{C}_p$
MELS (5)	$\mathbf{I}_{nxn}$	$\mathbf{0}_{mxm}$
MSLC (6)	$\mathbf{A}^T_{PB}\mathbf{A}_{PB}$	$\mathbf{A}^T_p\mathbf{S}^T\mathbf{S}\mathbf{A}_p$
MSPL (7)	$\mathbf{A}^T_{PB}\mathbf{R}_{PB}\mathbf{A}_{PB}$	$\mathbf{A}^T_p\mathbf{S}^T\mathbf{R}_p\mathbf{S}\mathbf{A}_p$

IV. RESULTS

A. Implementation

The control experiments were executed with Simulink RealTime interface on an Intel NUC PC with 2GB DDR-3 RAM and a Core i5-3427U processor (3M cache) running at 1.8 Ghz. The control algorithm is implemented and all sensor measurements are obtained at a sampling rate of 1kHz. A custom MATLAB implementation of the Goldfarb-Idnani method [26] is used to solve the strictly convex QP problem. Owing to hardware limits, we restricted the knee ESB tendon extension range and the maximum linear velocity of the ESB actuators in the QP problem to 0.072 m and 0.007 m/s. The elements of the weighting matrix $\tilde{\mathbf{W}}$ for the slack variables $\tilde{\mathbf{p}}$ are set such that they are at least two orders of magnitude higher than the elements of the quadratic term associated with $\mathbf{p}$.

The electrical power is computed using current measurements from the sensors in the actuators and including the back-EMF and the electrical dynamics. They are then integrated to yield the energy expenditure. Further, since untethered robots are equipped with power sources on-board, typically rechargeable Li-ion batteries and are capable of four quadrant operation, we consider negative power flows in our energy calculations.

B. Experiments

We first performed cyclic squat experiments wherein the cartesian position of the trunk is commanded to trace inclined elliptical trajectories of 0.3 Hz with horizontal and vertical amplitudes of 3 and 15 cm respectively. As the energy efficiency of the biarticular configuration has been established previously, the data from noESB configuration is not visually presented. For all the three cost functions, the ESB pretensions were initialized such that they accounted for the gravity torque at the initial configuration of the squat motions. Fig.4 displays the knee torque, actuator current and power and the total energy expenditure for the biarticulated configuration after the pretension references from the controller converge.

From the knee torque plots Fig.4a-4c, it can be observed that the joint torque distribution among the PB and ESB are different with the three criteria. While MELS criterion clearly allocates the maximum torque demand to the ESBs, MSLC and MSPL criteria converge to a similar strategy that demands lower torque from the ESB actuators. From Fig.4d-4f, the actuator current for the ankle ESB across all the cost functions are negligible. In comparison to MELS, MSLC and MSPL criteria demand considerable positive power from the ankle SEA, see Fig. 4g-4i. It is worth clarifying that while MSLC and MSPL minimize the current and power losses involved with the load torques alone, the plots depict currents and powers that include contributions necessary to overcome friction in the transmission units and drive the actuator inertias to the required accelerations. Furthermore, a slight chattering in the reference pretensions obtained from the QP solver with MSPL propagates in the current and power readings. However, MSPL criterion manages to

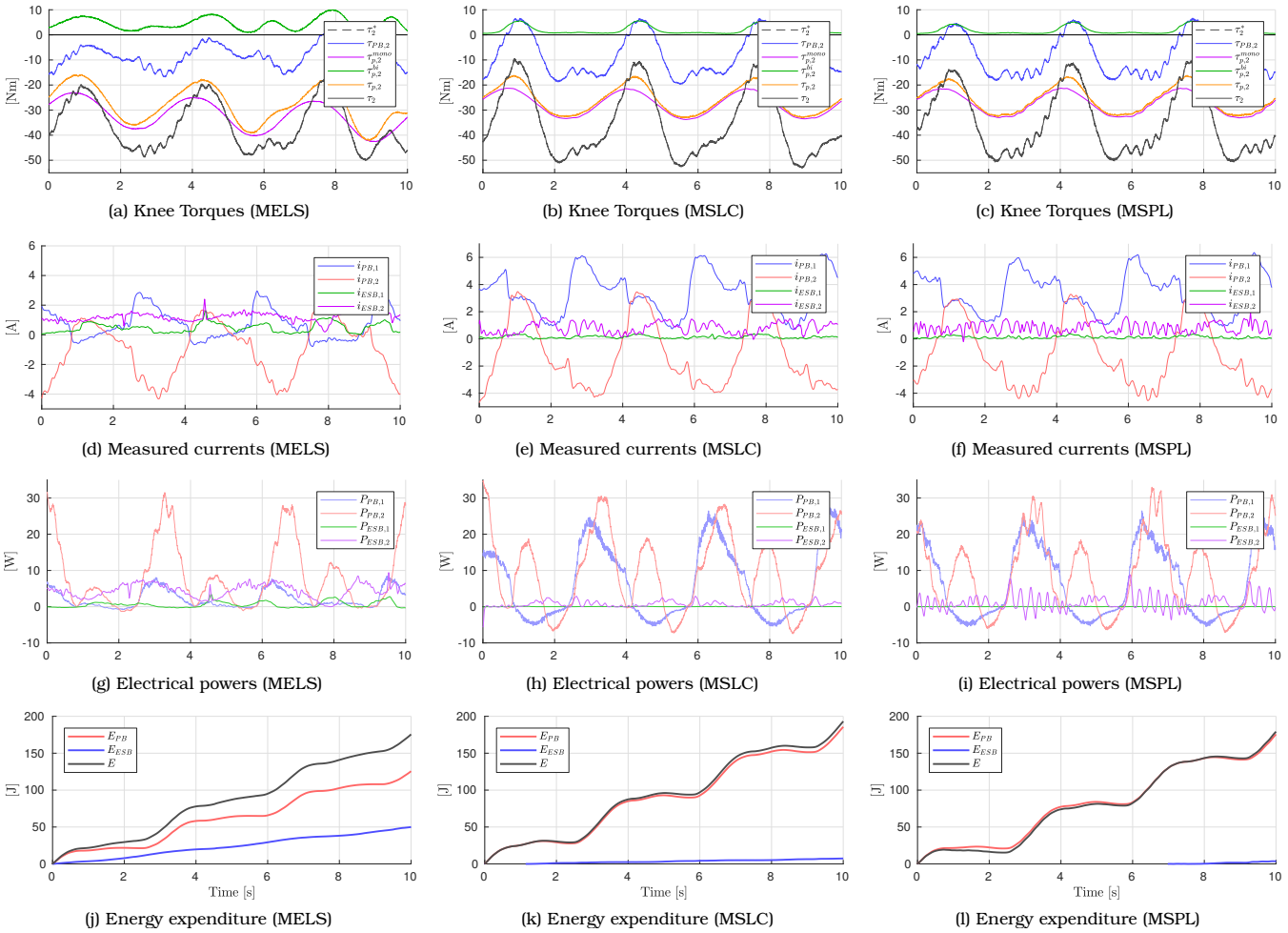

(a) Knee Torques (MELS) (b) Knee Torques (MSLC) (c) Knee Torques (MSPL)

(d) Measured currents (MELS) (e) Measured currents (MSLC) (f) Measured currents (MSPL)

(g) Electrical powers (MELS) (h) Electrical powers (MSLC) (i) Electrical powers (MSPL)

(j) Energy expenditure (MELS) (k) Energy expenditure (MSLC) (l) Energy expenditure (MSPL)

Fig. 4. Data from squat experiments (x-amp: 3 cm, y-amp: 15 cm). $(.)_1$, $(.)_2$ and $(.)_3$ correspond to quantities associated with the ankle, knee and hip joints respectively. Biarticulated configuration, left column : *Maximize ESB load share* (MELS), 184.3 J, middle column: *Minimize sum of squared load currents* (MSLC), 193.2 J, right column: *Minimize sum of power losses* (MSPL), 177.1 J. The noESB configuration consumes 598.66 J for the same squat motion. Associated energy savings are 69% (MELS), 67% (MSLC) and 70% (MSPL). The noESB results are redacted for reasons of space.

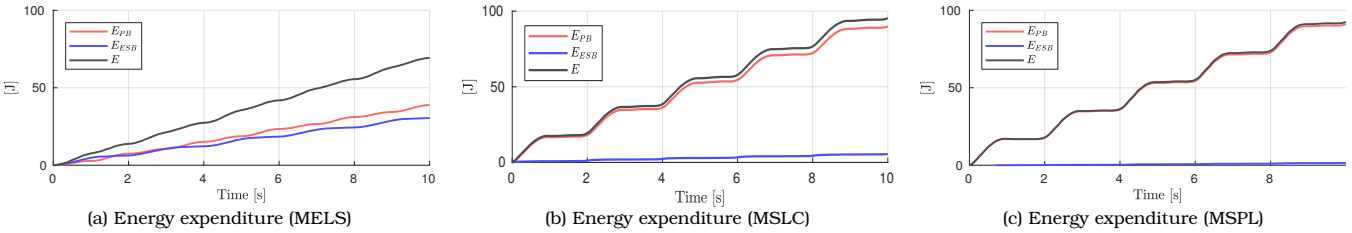

(a) Energy expenditure (MELS) (b) Energy expenditure (MSLC) (c) Energy expenditure (MSPL)

Fig. 5. Data from elliptical squat experiments (x-amp: 3 cm, y-amp: 6 cm, freq: 0.5Hz). Left column: MELS, 69.28 J, middle column: MSLC, 95.46 J, right column: MSPL, 92.56 J. The noESB configuration consumes 686 J to execute the same squat motion.

complete the squat motion with the least energy expenditure as can be seen from Fig. 4j-4l. Besides, it is interesting to observe the significant negative power phases with MSLC and MSPL criteria when the robot squats down. This occurs because the pretensions of the ESB tendons are smaller than when using the MELS criterion, so the required counter-action by the PBs to drive the leg in the "squat-down" phase is lower, leading to higher backdrivability of the PB actuators. Therefore, even if higher reference torques are demanded when driving against gravity, the reference torque demand drops by about 10 Nm during the other phases. Consequently, this phenomenon leads to almost negligible energy consumption during the "squat-down" phase and maintains on-par energy efficiency. The noESB configuration consumes 599 J, substantially higher than when biarticulated.

Thereupon, it also becomes essential to verify if the energy saved in a particular phase is higher than the extra energy spent in the other phase with the MSLC and the MSPL criteria. In a second set of experiments, to analyze the candidate criteria across frequencies, in the biarticulated configuration, the hip is commanded to track smaller amplitude squat trajectories (x-amplitude: 3 cm, y-amplitude: 6 cm)

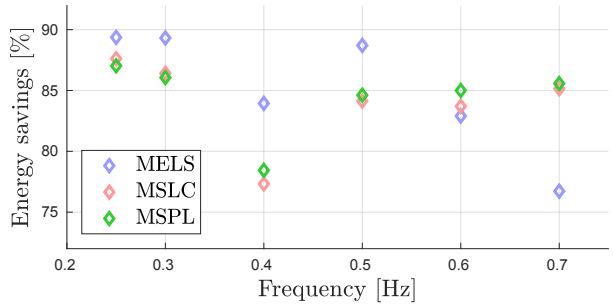

Fig. 6. Energy savings with the three criteria from squat experiments (x-amp: 3 cm, y-amp: 6 cm) for the biarticulated configuration with respect to the noESB configuration while the eLeg executes squats across frequencies.

at various frequencies. Owing to the limits of the actuator performance, experiments were performed only up to 0.7 Hz. Albeit smaller motions, they necessitate considerable torques especially at the knee joint, where the reference torque consistently exceeds the maximum continuous torque of the SEA. The observations made are two-fold. Firstly, at 0.5 Hz squats, similar inferences were made about the pretension references and gravity-driven phases. However, the MELS criterion seems to perform the same task more efficiently, see Fig. 5. Compared to the other two strategies, the excess energy that MELS entails in the "squat-down" phase is lower than the energy saved during the "squat-up" phase. Intuitively, since the torque reference variations are smaller than in the previous case, the knee PB had to oppose the ankle ESB lesser during "squat-down" phase, leading to higher overall efficiency. This result advocates for a case-by-case analysis for choice of a strategy with amplitude variations in trajectories. Further, the same will also depend on the relative dynamics of the PB and ESB actuators.

Secondly, we discuss about the energy savings across frequencies whose results are depicted in Fig.6. The energy savings obtained with the biarticulated configuration with respect to the noESB configuration are plotted across frequencies. It can been seen that at higher frequencies, the energy savings obtained with the MELS strategy, which relies on the maximum ESB utilization, drops below the savings of the other two criteria. Consequently, there is less opposition to the PB actuators being back-driven by the gravity potential. This is in line with the ESB characteristics as they cannot be pretensioned at velocities higher than 0.007 m/s and cannot account for the necessary ESB torque variations with the MELS at higher frequencies. Although the conclusion is obtained for the executed trajectory and the same may vary with amplitudes, we expect a similar trend in the variation of these efficiencies for squat motions. However, the crossover point, the frequency at which MSPL overtakes MELS in efficiency could vary with different amplitudes.

C. Discussion

Multi-articulated systems exhibit couplings wherein a particular joint torque is affected by the configuration of the other articulated joints. Therefore, it is not straightforward to resolve the joint torques among the various actuators. For that reason, we use an optimization scheme that provides pretension references based on the chosen criteria. The analysis is conducted on squat motions because legged locomotion in general involves cyclic motion such as walking, hopping, jumping etc. The analysis is made to verify if the MELS is the optimal criterion owing to the higher ESB efficiencies. A first set of experiments indicated that MSPL can perform equally well as the MELS by promoting backdrivability.

In order to extend the analysis, we additionally execute squat experiments across frequencies. While the MELS results in higher energy savings at low frequencies, the higher pretensioned biarticulated ESB also hamper the PBs from being back-driven at higher frequencies. Especially, the MSPL criterion brings about negligible energy costs through longer gravity-driven phases. Though not described explicitly, this behaviour naturally emerges out of the controller. The RMS value of the cartesian hip position tracking errors for all reported experiments, across various criteria and configurations are all below 5 mm.

At this juncture, it is also important to realize that the efficiency of torque generation varies between actuators and depends on the actuator inertia, friction in the transmission units, thermal fatigue of the actuators, etc. This efficiency measure is not a constant and it varies with temperature, loading, velocity, component wear, etc. For instance, the efficiency of CPL-20 HD varies between 45-88 % [27]. Nevertheless, we regard uniform efficiencies across all actuators in this work. Additionally, the motor torque constant decreases with thermal fatigue. A valuable extension would be to integrate the efficiencies and their thermal variations specifically in (6) and (7).

V. Conclusion and Outlook

In this paper, an analysis is conducted on the eLeg that is powered by modular ACA branches to identify energy-efficient joint torque distribution strategies. An optimization based controller is presented which upon using quadratic criteria can provide instantaneous reference pretensions for the parallel actuators. The energy-based analysis is conducted to check if delegating the maximum torque demand to the highly efficient ESBs is always the best strategy.

Observations from one set of cyclic squat experiments indicated that the MSPL by lengthening negative power phases attains comparable energy savings with MELS strategy. From another set of experiments where eLeg executes squats across a range of frequencies we find that at lower frequencies although MELS is more effective, MSLC and MSPL can result in better efficiencies at higher frequencies as MELS results in longer actuator-driven motion phases.

Future work would be to account for thermal efficiencies and plan for longer horizons in a model-predictive fashion and obtain optimized pretensions specific to periodic motion amplitudes and frequencies. During extended operations, demanding higher torques from the ESBs once the SEAs are fatigued may hold the key to enduring autonomy. Moreover, suitably simplifying and incorporating non-quadratic criteria such as joint work minimization into the presented framework might provide additional insights.

REFERENCES

[1] P. Hebert, M. Bajracharya, J. Ma, N. Hudson, A. Aydemir, J. Reid, C. Bergh, J. Borders, M. Frost, M. Hagman *et al.*, "Mobile manipulation and mobility as manipulationdesign and algorithms of robosimian," *Journal of Field Robotics*, vol. 32, no. 2, pp. 255–274, 2015.

[2] N. Paine, J. S. Mehling, J. Holley, N. A. Radford, G. Johnson, C.-L. Fok, and L. Sentis, "Actuator Control for the NASA-JSC Valkyrie Humanoid Robot: A Decoupled Dynamics Approach for Torque Control of Series Elastic Robots: Actuator Control for the NASA-JSC Valkyrie Humanoid Robot," *Journal of Field Robotics*, vol. 32, no. 3, pp. 378–396, May 2015.

[3] M. Hutter, C. Gehring, D. Jud, A. Lauber, C. D. Bellicoso, V. Tsounis, J. Hwangbo, K. Bodie, P. Fankhauser, M. Bloesch *et al.*, "Anymal-a highly mobile and dynamic quadrupedal robot," in *2016 IEEE/RSJ International Conference on Intelligent Robots and Systems (IROS)*. IEEE, 2016, pp. 38–44.

[4] D. F. B. Haeufle, M. D. Taylor, S. Schmitt, and H. Geyer, "A clutched parallel elastic actuator concept: Towards energy efficient powered legs in prosthetics and robotics," in *2012 4th IEEE RAS & EMBS International Conference on Biomedical Robotics and Biomechatronics (BioRob)*. Rome, Italy: IEEE, Jun. 2012, pp. 1614–1619.

[5] G. Mathijssen, D. Lefeber, and B. Vanderborght, "Variable Recruitment of Parallel Elastic Elements: SeriesParallel Elastic Actuators (SPEA) With Dephased Mutilated Gears," *IEEE/ASME Transactions on Mechatronics*, vol. 20, no. 2, pp. 594–602, Apr. 2015.

[6] Xin Liu, A. Rossi, and I. Poulakakis, "SPEAR: A monopedal robot with Switchable Parallel Elastic actuation," in *2015 IEEE/RSJ International Conference on Intelligent Robots and Systems (IROS)*. Hamburg, Germany: IEEE, Sep. 2015, pp. 5142–5147.

[7] A. Mazumdar, S. J. Spencer, C. Hobart, J. Salton, M. Quigley, T. Wu, S. Bertrand, J. Pratt, and S. P. Buerger, "Parallel Elastic Elements Improve Energy Efficiency on the STEPPR Bipedal Walking Robot," *IEEE/ASME Transactions on Mechatronics*, vol. 22, no. 2, pp. 898–908, Apr. 2017.

[8] N. G. Tsagarakis, H. Dallali, F. Negrello, W. Roozing, G. A. Medrano-Cerda, and D. G. Caldwell, "Compliant antagonistic joint tuning for gravitational load cancellation and improved efficient mobility," in *Humanoid Robots (Humanoids), 2014 14th IEEE-RAS International Conference on*. IEEE, 2014, pp. 924–929.

[9] G. J. van Ingen Schenau, "From rotation to translation : Constraints on multi-joint motions and the unique action of biarticulated muscles," *Human Movement Science*, vol. 8, no. 1, pp. 301–337, 1989.

[10] L. Gregoire, H. Veeger, P. Huijing, and G. van Ingen Schenau, "Role of Mono- and Biarticular Muscles in Explosive Movements," *International Journal of Sports Medicine*, vol. 05, no. 06, pp. 301–305, Dec. 1984.

[11] F. Iida, J. Rummel, and A. Seyfarth, "Bipedal walking and running with spring-like biarticular muscles," *Journal of Biomechanics*, vol. 41, no. 3, pp. 656–667, 2008.

[12] W. Roozing, Z. Li, D. G. Caldwell, and N. G. Tsagarakis, "Design Optimisation and Control of Compliant Actuation Arrangements in Articulated Robots for Improved Energy Efficiency," *IEEE Robotics and Automation Letters*, vol. 1, no. 2, pp. 1110–1117, Jul. 2016.

[13] W. Roozing, Z. Li, G. A. Medrano-Cerda, D. G. Caldwell, and N. G. Tsagarakis, "Development and Control of a Compliant Asymmetric Antagonistic Actuator for Energy Efficient Mobility," *IEEE/ASME Transactions on Mechatronics*, vol. 21, no. 2, pp. 1080–1091, Apr. 2016.

[14] W. Roozing, Z. Ren, and N. G. Tsagarakis, "An efficient leg with seriesparallel and biarticular compliant actuation: design optimization, modeling, and control of the eleg," *The International Journal of Robotics Research*, vol. 0, no. 0, p. 0278364919893762, 0. [Online]. Available: https://doi.org/10.1177/0278364919893762

[15] ——, "Design of a Novel 3-DoF Leg with Series and Parallel Compliant Actuation for Energy Efficient Articulated Robots," in *2018 IEEE International Conference on Robotics and Automation (ICRA)*. Brisbane, QLD: IEEE, May 2018, pp. 1–8.

[16] V. Salvucci, Y. Kimura, S. Oh, T. Koseki, and Y. Hori, "Comparing Approaches for Actuator Redundancy Resolution in Biarticularly-Actuated Robot Arms," *IEEE/ASME Transactions on Mechatronics*, vol. 19, no. 2, pp. 765–776, Apr. 2014.

[17] L. Baccelliere, N. Kashiri, L. Muratore, A. Laurenzi, M. Kamedula, A. Margan, S. Cordasco, J. Malzahn, and N. G. Tsagarakis, "Development of a human size and strength compliant bi-manual platform for realistic heavy manipulation tasks," in *2017 IEEE/RSJ International Conference on Intelligent Robots and Systems (IROS)*. IEEE, 2017, pp. 5594–5601.

[18] Z. Ren, W. Roozing, and N. Tsagarakis, "The eLeg: A Novel Efficient Leg Prototype Powered by Adjustable Parallel Compliant Actuation Principles," in *2018 IEEE-RAS International Conference on Humanoid Robots (Humanoids)*. Beijing, CHN: IEEE, Nov. 2018, p. 7.

[19] W. Roozing, "Modeling and Control of Adjustable Articulated Parallel Compliant Actuation Arrangements in Articulated Robots," *Frontiers in Robotics and AI*, vol. 5, Feb. 2018.

[20] C. D. Remy, K. Buffinton, and R. Siegwart, "Comparison of cost functions for electrically driven running robots," in *2012 IEEE International Conference on Robotics and Automation*. St Paul, MN, USA: IEEE, May 2012, pp. 2343–2350.

[21] S.-H. Lee and A. Goswami, "A momentum-based balance controller for humanoid robots on non-level and non-stationary ground," *Autonomous Robots*, vol. 33, no. 4, pp. 399–414, Nov. 2012.

[22] M. Posa, S. Kuindersma, and R. Tedrake, "Optimization and stabilization of trajectories for constrained dynamical systems," in *2016 IEEE International Conference on Robotics and Automation (ICRA)*. Stockholm, Sweden: IEEE, May 2016, pp. 1366–1373.

[23] S. Kuindersma, F. Permenter, and R. Tedrake, "An efficiently solvable quadratic program for stabilizing dynamic locomotion," in *2014 IEEE International Conference on Robotics and Automation (ICRA)*. Hong Kong, China: IEEE, May 2014, pp. 2589–2594.

[24] S. P. Boyd and L. Vandenberghe, *Convex optimization*. Cambridge, UK ; New York: Cambridge University Press, 2004.

[25] S. Seok, "Actuator design for high speed proprioceptive control in fast legged locomotion," in *Intelligent Robots and Systems (IROS), 2012 IEEE/RSJ International Conference on*. Vilamoura, Portugal: IEEE, 2012, oCLC: 777811617.

[26] D. Goldfarb and A. Idnani, "A numerically stable dual method for solving strictly convex quadratic programs," *Mathematical Programming*, vol. 27, no. 1, pp. 1–33, Sep. 1983.

[27] "Harmonic Drive AG, Engineering Data, CPL-2A component sets," https://harmonicdrive.de/mage/media/catalog/category/05_05_CPL_2A_1.pdf, Accessed: 2019-08-30.